HARDWARE AND INSTRUMENTATION – Note

Magnetic Resonance in Medicine 66:605–608 (2011)

Relaxivity of Gadolinium Complexes Detected by Atomic Magnetometry

David J. Michalak,[1†] Shoujun Xu,[1‡] Thomas J. Lowery,[2§] C. W. Crawford,[1] Micah Ledbetter,[3] Louis-S. Bouchard,[1¶] David E. Wemmer,[2] Dmitry Budker,[3] and Alexander Pines[1*]

Laser atomic magnetometry is a portable and low-cost yet highly sensitive method for low magnetic field detection. In this work, the atomic magnetometer was used in a remote-detection geometry to measure the relaxivity of aqueous gadolinium-diethylenetriamine pentaacetic acid Gd(DTPA) at the Earth's magnetic field (40 μT). The measured relaxivity of 9.7 ± 2.0 s^{-1} mM^{-1} is consistent with field-cycling experiments measured at slightly higher magnetic fields, but no cryogens or strong and homogeneous magnetic field were required for this experiment. The field-independent sensitivity of 80 fT $Hz^{-1/2}$ allowed an in vitro detection limit of ~ 10 μM Gd(DTPA) to be measured in aqueous buffer solution. The low detection limit and enhanced relaxivity of Gd-containing complexes at Earth's field motivate continued development of atomic magnetometry toward medical applications. Magn Reson Med 66:605–608, 2011. © 2011 Wiley-Liss, Inc.

Key words: atomic magnetometry; relaxivity; gadolinium

The ability to selectively enhance the contrast of soft tissue in magnetic resonance imaging (MRI) distinguishes it from other biomedical imaging modalities (1,2). Gadolinium complexes, such as the broadly used Gd(DTPA), decrease the spin-lattice relaxation time (T_1) of nearby water, which alters the signal strength and increases medical imaging contrast for diagnostic purposes (3,4). The rate constant for nuclear spin relaxation per unit concentration of agent (termed relaxivity) of water protons in the presence of Gd(DTPA) is about 3.8 s^{-1} mM^{-1} at the magnetic fields typical for imaging (>1 T). To minimize the recently documented negative side effects of Gd(DTPA) (5), higher relaxivity values are desired to reduce dose without compromising image contrast. Conjugation of gadolinium to large molecules has been used to increase relaxivity but lower cellular uptake and altered clearance rates can result (6,7). Decreasing the magnetic field below 0.1 T enhances the relaxivity of unconjugated Gd agents (3,4), but the sensitivity of conventional inductive detection is poor at these fields. Both superconducting quantum interference devices and atomic magnetometry have good sensitivity at low magnetic fields and can be used as alternative detection techniques.

Low-field MRI has another diagnostic advantage: patients with metallic and/or magnetic implants (e.g., joint replacements, cochlear implants, pacemakers, or shrapnel) cannot be easily or safely imaged using conventional techniques. Because it requires no cryogens and relatively low power to operate, atomic magnetometry also has the unique advantage of portability. Thus, development of a portable Earth's magnetic field scanner could provide diagnosis at remote field sites or battlefields for subjects that cannot receive conventional MRI.

In this work, we report the measurement of Gd(DTPA) relaxivity at Earth's field using the optical atomic magnetometer (8–10) in a remote detection geometry (11). Conventional inductive detection would have the magnets necessary for polarization and the coils used for both encoding and detection located in near proximity. In the remote detection geometry, each of these regions can be physically separated. In this manner, the magnetic fields needed for prepolarizing the water can be physically separated from the sensitive detectors and the hardware used for encoding (e.g., spatial (12), velocity (13), or chemical shift (14) etc).

MATERIALS AND METHODS

The experimental setup is described in Fig. 1. Specifically, a buffered aqueous Gd(DTPA) solution is first polarized to equilibrium magnetization in a 0.6-T magnetic field; this field is generated by permanent magnets and may have low homogeneity as it is not needed for spatial encoding. The prepolarizing field provides a starting magnetization, M_0, for measuring the relaxation rates at Earth's field in the presence of Gd(DTPA). The

[1]Materials Sciences Division, Lawrence Berkeley National Laboratory, Department of Chemistry, University of California, Berkeley, California, USA.
[2]Physical Biosciences Division, Lawrence Berkeley National Laboratory, Department of Chemistry, University of California, Berkeley, California, USA.
[3]Nuclear Sciences Division, Lawrence Berkeley National Laboratory, Department of Physics, University of California, Berkeley, California, USA.
[†]*Present address:* Components Research, Intel Corporation, Hillsboro, OR 97124.
[‡]*Present address:* Department of Chemistry, University of Houston, Houston, TX 77204.
[§]*Present address:* T2 Biosystems, 286 Cardinal Medeiros Ave, Cambridge, MA 02141.
[¶]*Present address:* Department of Chemistry and Biochemistry, California NanoSystems Institute, Biomedical Engineering IDP, and Jonsson Comprehensive Cancer Center, University of California, 607 Charles E. Young Dr. East Los Angeles, CA 90095.

Grant sponsor: U.S. Department of Energy, Office of Basic Energy Sciences, Division of Materials Sciences and Engineering; Grant number: DE-AC02-05CH11231; Grant sponsors: ONR MURI grant and Nuclear Sciences Division of the U.S. Department of Energy

*Correspondence to: Alexander Pines, Ph.D., Materials Sciences Division, Lawrence Berkeley National Laboratory, Department of Chemistry, University of California, Berkeley, California, USA. E-mail: pines@berkeley.edu

Received 4 June 2010; revised 6 December 2010; accepted 12 December 2010.
DOI 10.1002/mrm.22811
Published online 23 March 2011 in Wiley Online Library (wileyonlinelibrary.com).

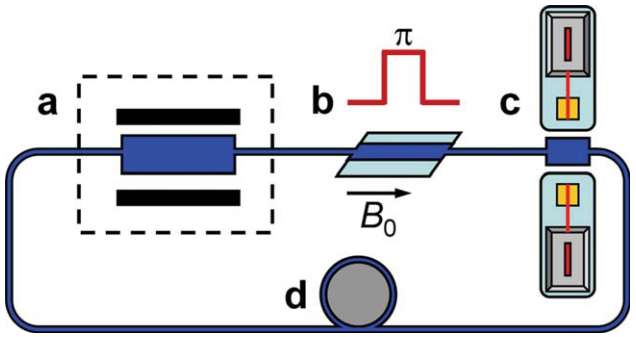

FIG. 1. Description of the experimental schematic: (**a**) the prepolarization region, which consists of a pair of permanent magnets (black rectangles) to provide a 0.6 T field and 15 mL reservoir (blue square); (**b**) the encoding region where B_0 = Earth-field and a saddle-type coil is used to invert the nuclear spins; (**c**) the detection region is comprised of two atomic-magnetometers to eliminate common mode noise; and (**d**) variable-speed peristaltic pump to change the speed of liquid transport from the prepolarizer to the detector. The Gd(DTPA) solution is indicated in blue.

prepolarized solution subsequently flows out of the 0.6-T prepolarizing field adiabatically into a 400-μL encoding region in the Earth's magnetic field (~40 μT in our laboratory). A π pulse (1.6 kHz, 2.4 msec) is applied using a saddle coil (oriented relative to the direction of the Earth's field in our laboratory) to invert the nuclear spins within the encoding region. This encoding distinguishes these spins from neighboring spins in the flowing solution. The encoded solution subsequently flows into a 400-μL detection region adjacent to the magnetometer, which has a low-frequency (0.1 Hz) sensitivity of 80 fT $Hz^{-1/2}$ as detailed in previous publications (8–10). The magnetometer detects the difference in magnetization between the inverted spins and the noninverted spins: $M_{measured} = M - (-M) = 2M$, where $M_{measured}$ is the signal from the magnetometer and M is sample magnetization which depends on the amount of spin relaxation. The detected magnetization is thus divided by 2 to calculate the sample magnetization.

The relaxation rate of hydrogen nuclei is measured by varying the time (termed "evolution time") between prepolarization and detection by using a variable-speed peristaltic pump. The 0.6-T prepolarization volume was sufficiently large (~ 15 mL) to allow a residence time of at least 10 T_1 for all pumping speeds; this is needed to ensure that the nuclear spins achieve equilibrium magnetization within the prepolarization region even for the fastest pump rate. Under these conditions, all solutions containing various Gd(DTPA) concentrations leave the prepolarization region with the same initial magnetization, M_0, and the sample magnetization, M, measured at the detector is only due to Earth's field decay rates in the presence of Gd(DTPA) rather than insufficient prepolarization.

RESULTS

Six Gd(DTPA) concentrations in a 10 mM phosphate buffer solution (used for biological relevance) were studied: 0 (buffer only), 1, 5, 10, 20, and 50 μM. The decay curves of sample magnetization ($M = M_{measured}/2$) vs. evolution time for each Gd(DTPA) concentration are presented in Fig. 2. The magnetization of a given Gd(DTPA) solution, M, after time, t, can be related to the initial magnetization, M_0, and the relaxation rate ($1/T_1$) by Eq. 1:

$$M = M_0 \exp\left[-\frac{1}{T_1}t\right] \quad [1]$$

Thus, a linear fit to ln(M) vs. t gives a y-intercept of ln(M_0) and a slope of $-1/T_1$. The colored solid lines of Fig. 2 are the linear regressions to the data, and the M_0 values obtained from linear regressions of each Gd(DTPA) concentration are similar, as expected for the constant prepolarization field; the range in M_0 values is only ~ 5% of the mean. The decay profiles for the 1 and 5 μM Gd(DTPA) solutions show very little difference from the buffer, but noticeably faster decay rates were observed for Gd(DTPA) concentrations of 10 μM and greater. This detection limit of ~ 10 μM is quite a bit lower than the reported values for Gd(DTPA) complexes at clinical fields (> 50 μM) (15,16). Figure 3 plots the calculated relaxation rates ($1/T_1$ values) for each Gd(DTPA) concentration. The relaxivity of Gd(DTPA) can be calculated from Eq. 2 (3,4)

$$\frac{1}{T_1} = \frac{1}{T_1(0)} + \alpha C \quad [2]$$

where $T_1(0)$ is the relaxation rate observed for the buffer only, α is the relaxivity, and C is the concentration of Gd(DTPA). The slope of a linear fit to $1/T_1$ vs. Gd(DTPA) concentration results in an Earth's-field relaxivity value of 9.7 ± 2.0 s^{-1} mM^{-1}, which is within error of the ~ 7.8 s^{-1} mM^{-1} relaxivity obtained from field-cycling measurements at low fields (0.1–20 mT) (3,4).

DISCUSSION AND CONCLUSIONS

These results of our relaxivity experiment are important for two reasons. First, to our knowledge, this is the first

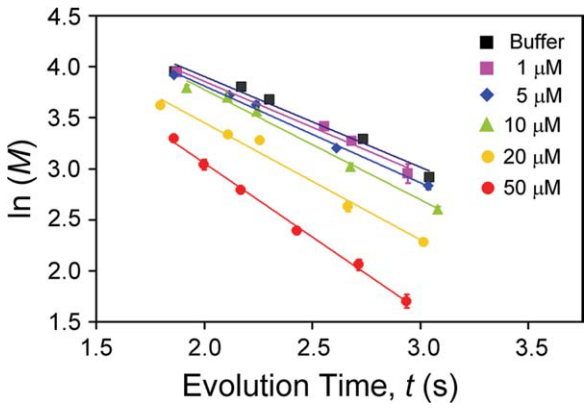

FIG. 2. Plot of ln(M) vs. time in Earth's field between prepolarization and detection; M is the detected magnetization (in units of 10^{-13} T). Solid colored lines are linear fits to the data used with Eq. 1 to obtain a $1/T_1$ value for each Gd(DTPA) concentration.

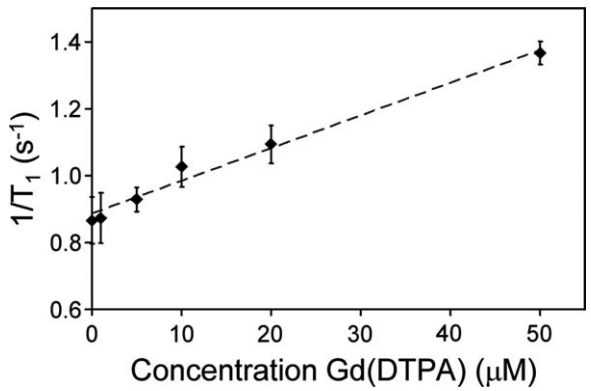

FIG. 3. Plot of $1/T_1$ vs. Gd(DTPA) concentration. The dashed line is a linear fit of the data to Eq. 2. The slope of the linear regression gives a relaxivity value of $9.7 \pm 2.0\ s^{-1}\ mM^{-1}$.

reported measurement of the relaxivity of Gd(DTPA) complexes at magnetic fields as low at 40 μT (Earth's field). Second, the sensitivity of the magnetometer is sufficient to detect small changes in Gd(DTPA) concentration with a detection limit of $\sim$ 10 μM. This detection limit is due to both the higher relaxivity of aqueous Gd(DTPA) at low field and the excellent sensitivity of the atomic magnetometer at low field.

Although continued development of this technique is needed to produce contrast-enhanced images of diagnostic quality, the results show progress in the application of atomic magnetometers to the field of medicine. Atomic magnetometry has already demonstrated MRI for fluid flow in various phantoms (10,17), but the uniqueness of this approach is highlighted by recent MR imaging in the presence of metals (12). This is achieved through the excellent sensitivity at low magnetic fields, where skin depth and susceptibility differences are less severe. Since the sensitivity of atomic magnetometry only outperforms inductive detection at magnetic fields less than conventional detection (18), it should not be considered as a competitor to conventional inductive detection. Rather, atomic magnetometry should be considered as a complementary tool for diagnosis of patients with cardiac pacemakers, artificial joints, insulin pumps, or shrapnel wounds who cannot receive conventional MRI diagnosis.

Atomic magnetometers have a significant cost advantage over conventional MRI systems; the optical detectors (no cryogens) and relaxed homogeneity of the prepolarization field present major cost savings. When used in the remote-detection geometry as described in this work, the atomic magnetometer could present a cost-effective method for relaxivity screening of various biofluids, such as contrast agent detection in urine, or for blood serum screening as a diagnostic (19) or as quality control during transfusions (20).

Potential in vivo applications of remote detection are angiography for which blood flow around constrictions is naturally suited to remote detection. In this geometry, a portable sensor containing coils for prepolarization and one-sided gradients would be coupled with the atomic magnetometer cells. The atomic magnetometer is, however, not limited to remote detection geometries; nanoparticle detection (21) and magneto-encephalography (22) have been demonstrated. Direct imaging with atomic magnetometry is more complicated due to the r^{-3} scaling of the magnetometer cells. Our calculations suggest that a surface scanner that generates a low 300-mT prepolarization field equipped with an rf magnetometer of 1 fT $Hz^{-1/2}$ sensitivity (23) can generate a 32×32 image with voxel size of $2.2 \times 2.2 \times 2.2\ mm^3$ at 1 cm depth with signal-to-noise ratio of $\sim$ 50 in 12 min. Imaging of deep tissue would result in significantly larger voxel sizes, but surrounding the subject with multiple magnetometers in a helmet or tube geometry could gain performance. Although the estimated imaging performance is not nearly competitive with clinical technologies, the possibility of low-field imaging coupled with portability demonstrates the relevance of atomic magnetometry as a complementary technique. The results presented here thus motivate further research and development of atomic magnetometers toward biomedical applications. On the basis of portability, cost, and recent Earth's field imaging results (8–10), we expect that ultra low-field, laser-detected microfluidic rapid-screening and/or contrast-enhanced MRI images will be useful in future medical applications.

ACKNOWLEDGMENTS

Research was supported by the U.S. Department of Energy, Office of Basic Energy Sciences, Division of Materials Sciences and Engineering under Contract No. DE-AC02-05CH11231 [Dr. Michalak, Dr. Xu, Dr. Crawford, Dr. Bouchard, and Dr. Pines], by the Nuclear Sciences Division of the U.S. Department of Energy, and by an ONR MURI grant.

REFERENCES

1. Hendee WR. Medical imaging physics. New York: Wiley; 2002.
2. Weinmann H-J, Ebert W, Misselwitz B, Schmitt-Willich H. Tissue-specific MR contrast agents. Eur J Radiol 2003;46:33–44.
3. Caravan P. Strategies for increasing the sensitivity of gadolinium based MRI contrast agents. Chem Soc Rev 2006;35:512.
4. Koenig S. From the relaxivity of Gd(DTPA)2- to everything else. Magn Reson Med 1991;22:183–190.
5. Kuo PH, Kanal E, Abu-Alfa AK, Cowper SE. Gadolinium-based MR contrast agents and nephrogenic systemic fibrosis. Radiology 2007; 242:647–649.
6. Allen MJ, MacRenaris KW, Venkatasubramanian PN, Meade TJ. Cellular delivery of MRI contrast agents. Chem Biol 2004;11:301–307.
7. Mulder WJM, Strijkers GJ, van Tilborg GAF, Griffioen AW, Nicolay K. Lipid-based nanoparticles for contrast-enhanced MRI and molecular imaging. NMR Biomed 2006;19:142–164.
8. Budker D, Romalis MV. Optical magnetometry. Nat Phys 2007;3: 227–234.
9. Xu S, Rochester SM, Yashchuk VV, Donaldson MH, Budker D. Construction and applications of an atomic magnetic gradiometer based on nonlinear magneto-optical rotation. Rev Sci Instrum 2006;77:083106.
10. Xu SJ, Yashchuk VV, Donaldson MH, Rochester SM, Budker D, Pines A. Magnetic resonance imaging with an optical atomic magnetometer. Proc Nat Acad Sci USA 2006;103:12668–12671.
11. Harel E, Granwehr J, Seeley JA, Pines A. Multiphase imaging of gas flow in a nanoporous material using remote-detection NMR. Nat Mater 2006;5:321–327.
12. Xu S, Harel E, Michalak DJ, Crawford CW, Budker D, Pines A. Flow in porous metallic materials: a magnetic resonance imaging study. J Magn Reson Imaging 2008;28:1299–1302.
13. Paulsen J, Bajaj VS, Pines A. Compressed sensing of remotely detected MRI velocimetry in microfluidics. J Magn Reson 2010;205: 196–201.

14. Harel E, Pines A. Spectrally resolved flow imaging of fluids inside a microfluidic chip with ultrahigh time resolution. J Magn Reson 2008; 193:199–206.
15. Hanaoka K, Lubag AJM, Castillo-Muzquiz A, Kodadek T, Sherry AD. The detection limit of Gd3+-based T1 agents is substantially reduced when targeted to a protein microdomain. Magn Reson Imaging 2008; 26:608–617.
16. Langereis S, de Lussanet QG, van Genderen MHP, Meijer EW, Beets-Tan RGH, Griffioen AW, van Engelshoven JMA, Backes WH. Evaluation of Gd(III)DTPA-terminated poly(propylene imine) dendrimers as contrast agents for MR imaging. NMR Biomed 2006;19: 133–141.
17. Xu S, Crawford CW, Rochester SM, Yashchuk VV, Budker D, Pines A. Submillimeter-resolution magnetic resonance imaging at the Earth's magnetic field with an atomic magnetometer. Phys Rev A 2008;78:013404.
18. Savukov IM, Seltzer SJ, Romalis MV. Detection of NMR signals with a radio-frequency atomic magnetometer. J Magn Reson 2007;185:214–220.
19. Blicharska B, Witek M, Fornal M, MacKay AL. Estimation of free copper ion concentrations in blood serum using T1 relaxation rates. J Magn Reson 2008;194:41–45.
20. Salo S, Alanen A, Leino R, Bondestam S, Komu M. The effect of haemosiderosis and blood transfusions on the T2 relaxation time and 1/T2 relaxation rate of liver tissue. Br J Radiol 2002;75:24–27.
21. Xu S, Donaldson MH, Pines A, Rochester SM, Budker D, Yashchuk VV. Application of atomic magnetometry in magnetic particle detection. Appl Phys Lett 2006;89:224105.
22. Xia H, Baranga AB-A, Hoffman D, Romalis MV. Magnetoencephalography with an atomic magnetometer. Appl Phys Lett 2006;89:211104.
23. Lee SK, Sauer KL, Seltzer SJ, Alem O, Romalis MV. Subfemtotesla radio-frequency atomic magnetometer for detection of nuclear quadrupole resonance. Appl Phys Lett 2006;89:214106.